

# Silica-supported aminoxyls as reactive materials for NO<sub>x</sub> removal†

Tatiana Luts, Enrique Iglesia\* and Alexander Katz\*

Received 26th August 2010, Accepted 18th October 2010

DOI: 10.1039/c0jm02826f

The design of new materials for gaseous NO<sub>x</sub> (NO and NO<sub>2</sub>) removal at ambient temperature using organic active sites is reported. The materials consist of unfunctionalized silica and silica modified by immobilized aminoxyls and function *via* sequential processes consisting of (i) NO oxidation to NO<sub>2</sub> and (ii) NO<sub>2</sub> storage. NO<sub>x</sub> removal by physical mixtures of immobilized PTIO (2-phenyl-4,4,5,5-tetramethyl-imidazoline-3-oxide-1-oxyl) sites on silica as the NO oxidant and hydrated silica as the NO<sub>2</sub> trap occurs with significant degradation of the PTIO oxidant *via* undesired side reactions with NO<sub>2</sub> when NO<sub>2</sub> adsorption sites are fewer than required for its complete removal along the packed bed. The use of packed beds with sufficient NO<sub>2</sub> adsorption sites requires a large excess of unfunctionalized silica, because of its low surface density of geminal silanols, which are shown to be the relevant sites for NO<sub>2</sub> storage on silica at ambient temperature based on density functional theory calculations. This PTIO degradation is circumvented by the design of NO<sub>x</sub> traps consisting of immobilized PTIO on silica as the NO oxidant and immobilized TEMPO (2,2,6,6-tetramethylpiperidine-1-oxyl) on silica as an adsorbent with a high density of strong NO<sub>2</sub> binding sites. Packed beds consisting of a 2 : 1 molar mixture of PTIO and TEMPO sites consume NO<sub>x</sub> as predicted by stoichiometry without detectable PTIO degradation and also without a contribution from geminal silanols as NO<sub>2</sub> storage sites. This result requires that PTIO and TEMPO sites on silica render geminal silanols as inactive towards NO<sub>2</sub> storage presumably because of the titration of these silanols by immobilized aminoxyls.

## Introduction

The application of cascade reactions is an emerging research area that spans synthetic<sup>1,2</sup> and biological<sup>3,4</sup> catalysts, and has the potential to integrate the unique properties of both types of catalysts within a single process.<sup>5–7</sup> Chemical syntheses *via* single-pot cascade reactions can substantially increase selectivity by circumventing the need for multiple steps and separations in sequential reactions, or by reacting unstable intermediates near sites on which they are formed. The diverse applications of cascade reactions enable production of fine chemicals,<sup>8</sup> polymers,<sup>1</sup> and biofuels,<sup>9,10</sup> using both heterogeneous and homogeneous catalysts. Synergies among active sites on solid supports strongly influence rates and selectivities, as shown recently for sequential reaction systems involving cooperative active site pairs, such as thiol/sulfonic acid sites for bisphenol-A synthesis,<sup>11</sup> acid/base bifunctional sites for aldol-related catalysis,<sup>12–14</sup> Au(0)/Ti(IV)<sup>15–18</sup> for olefin epoxidation, and supported Pt/BaO for NO<sub>x</sub> (NO and NO<sub>2</sub>) storage.<sup>19,20</sup>

Here, we describe the design of materials for NO<sub>x</sub> removal at ambient temperature based on cascade reactions consisting of NO oxidation and NO<sub>2</sub> storage on two different active sites (labeled A and B), as shown in Scheme 1a. The applications of such materials for NO<sub>x</sub> adsorption include tobacco smoke filters,<sup>21</sup> low-temperature storage components for NO<sub>x</sub> abatement from engine effluents,<sup>22</sup> NO removal for controlling

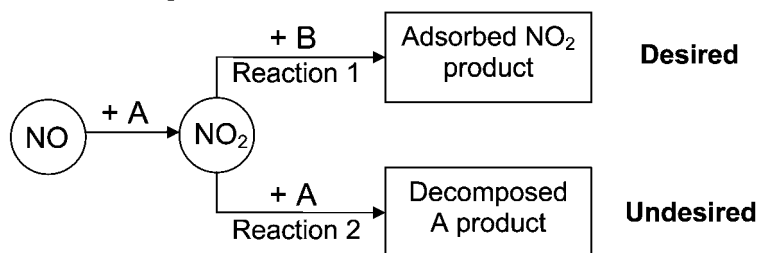
signaling in mammalian cells,<sup>23</sup> and atmospheric chemistry studies.<sup>24</sup> The particular active sites used here consist of silica-supported organic radicals and unfunctionalized silica surfaces, as represented in Scheme 1b. Site A in Scheme 1a consists of 2-phenyl-4,4,5,5-tetramethyl-imidazoline-3-oxide-1-oxyl (PTIO), which has been previously shown to react with NO to form NO<sub>2</sub> and 2-phenyl-4,4,5,5-tetramethyl-imidazoline-3-oxide (PTI).<sup>25–28</sup> Site B in our study is represented by either inorganic silica surface species (B<sub>1</sub>), which react with NO<sub>2</sub> to form either a combination of NO and HNO<sub>3</sub><sup>29–31</sup> or adsorbed N<sub>2</sub>O<sub>4</sub>,<sup>32–34</sup> or by organic aminoxyl 2,2,6,6-tetramethylpiperidine-1-oxyl (TEMPO = B<sub>2</sub>) species, both of which are shown in Scheme 1b. TEMPO reacts with two NO<sub>2</sub> to form NO and oxoammonium nitrate of TEMPO *via* a short-lived nitrite intermediate as shown in Scheme 1b.<sup>35–37</sup> Both PTIO and TEMPO are known to be stable with regard to ambient oxygen and water, and therefore can be utilized without air-free treatment.<sup>38</sup>

Our principal objective is to examine how materials consisting of mixtures of type A and B sites function for NO<sub>x</sub> storage with specific emphasis on the requirements for selective NO<sub>x</sub> adsorption when using silica-supported aminoxyl sites. We investigate NO<sub>x</sub> removal in materials composed of different concentrations of PTIO within a matrix of B-type sites. This is performed by treating materials consisting of different proportions of type A and B sites with flowing streams containing NO or NO<sub>2</sub> while measuring their concentrations with an infrared gas analyzer. A crucial aspect of this study is to elucidate the role of B<sub>1</sub>-type sites for NO<sub>x</sub> storage in the presence of immobilized aminoxyl species on silica support, and specifically, whether immobilized aminoxyls titrate B<sub>1</sub>-type sites. Another important issue concerns the

Department of Chemical and Biomolecular Engineering, University of California at Berkeley, Berkeley, CA, 94720, USA. E-mail: igelesia@berkeley.edu; askatz@berkeley.edu; Fax: +1 510 642 4778

† Electronic supplementary information (ESI) available: Further details. See DOI: 10.1039/c0jm02826f

## a) Schematic representation



NO/PTIO stoichiometry ( $S$ ) is a fraction of A-site reacted *via* desired pathway and is equal to NO oxidized to NO<sub>2</sub> per PTIO.

## b) Specific reagents and reactions

Active site	Reaction	NO <sub>2</sub> consumed per NO formed ( $\chi$ )
$A =$ PTIO	$+ NO \rightarrow$ PTI + NO <sub>2</sub>  $+ 2 NO_2 \rightarrow$ oxoammonium PTIO nitrate + NO	N/A  2
$B_1 =$ silica-1073	$+ 2 NO_2 \rightarrow$ N <sub>2</sub> O <sub>4</sub> on silica-1073	$\infty$
	$\downarrow + NO_2$ 2 HNO <sub>3</sub> on silica-1073 + NO	3
$B_2 =$ TEMPO	$+ 2 NO_2 \rightarrow$ oxoammonium TEMPO nitrate + NO	2

**Scheme 1** Cascade reaction scenario, wherein intermediates formed can degrade reactant active site.

potential involvement of undesired side reactions of A-type sites in the presence of gas phase NO<sub>2</sub>. The understanding gained in this study and the evidence presented herein enable the design and synthesis of materials for NO<sub>x</sub> storage at ambient temperature based on purely organic active sites, consisting of

immobilized PTIO and TEMPO sites. These materials are shown to function as selective NO<sub>x</sub> adsorbents and to obey the expected stoichiometry for the organic active sites without detectable side reactions and without involvement of inorganic binding species for NO<sub>x</sub> storage.

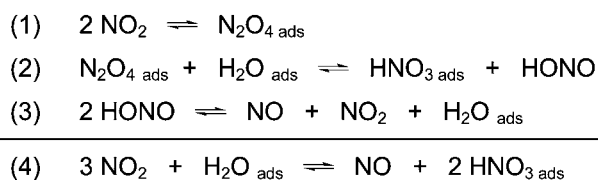
## Results and discussion

### 1. NO<sub>2</sub> adsorption by B<sub>1</sub> sites (silica-1073)

The interactions of NO<sub>2</sub> with silicon oxide surfaces have been the subject of several investigations because of their relevance in atmospheric chemistry, as well as in adsorption and heterogeneous catalysis.<sup>29–34,39,40</sup> NO<sub>2</sub> adsorption on silica occurs at near ambient temperature and has been proposed to involve N<sub>2</sub>O<sub>4</sub> as the surface-bound species.<sup>32–34</sup> The adsorbed dimer can react with physisorbed H<sub>2</sub>O on silica to form nitric acid (HNO<sub>3</sub>) and nitrous acid (HONO),<sup>29–31</sup> which can further decompose to NO and NO<sub>2</sub><sup>41</sup> according to the reaction sequence shown in Scheme 2.

Silica-1073 in its hydrated (silica-1073 exposed to ambient moisture) and anhydrous (silica-1073 without exposure to ambient atmosphere) forms was examined as a NO<sub>2</sub> adsorbent because silica-1073 is used here as support for aminoxyl species. During exposure of anhydrous silica-1073 to NO<sub>2</sub> ( $8 \times 10^{-8}$  mol NO<sub>2</sub> (g-silica s)<sup>-1</sup>), no nitrogen-containing species were detected in the effluent up to a saturation capacity of 65 μmol NO<sub>2</sub> g-silica<sup>-1</sup> (0.1 NO<sub>2</sub> nm<sup>-2</sup>). The assumption of dimers as the adsorbed species,<sup>32–34</sup> as suggested by the non-oxidative adsorption step (1) in Scheme 2, gives an adsorption site density of 0.05 N<sub>2</sub>O<sub>4</sub> nm<sup>-2</sup>. This site density is much smaller than the total silanol coverage of silica-1073 (0.7 OH nm<sup>-2</sup>) and resembles the geminal site densities reported on silica-1073 (0.1 OH nm<sup>-2</sup>; 0.05 Si(OH)<sub>2</sub>).<sup>42</sup> This suggests that geminal silanols may act as the binding sites for N<sub>2</sub>O<sub>4</sub> adsorption on anhydrous silica-1073 at ambient temperature.

This proposal was supported by density functional theory calculations using the B3LYP functional with a 6-311 + G(d,p) basis set. Fig. 1 displays the final optimized geometry of N<sub>2</sub>O<sub>4</sub> interactions with Si<sub>4</sub>O<sub>11</sub>H<sub>6</sub> molecular cluster used as the model for the silica surface. This cluster allows a direct comparison of isolated and geminal silanol sites in internally consistent calculations. The optimized geometry shows two significant interactions between geminal silanols and adsorbed N<sub>2</sub>O<sub>4</sub>: (i) a dominant electrostatic interaction involving one of the geminal silanol O-atom lone pairs and the N-atoms of N<sub>2</sub>O<sub>4</sub>, which is evidenced by a O...N distance of 2.9 Å (equidistant for both N-atoms), and (ii) a secondary hydrogen bond interaction involving the other geminal silanol and one of the negatively charged O-atom of N<sub>2</sub>O<sub>4</sub>, which is evidenced by a O–H...O distance of 3.2 Å. Only a geminal silanol site provides the ability for both interactions (i) and (ii) above and results in an energy-optimized heat of adsorption of 17.1 kJ mol<sup>-1</sup>. These results are consistent with previous calculations of N<sub>2</sub>O<sub>4</sub> adsorption on molecular models of silica, which demonstrate a stronger binding energy using Si(OH)<sub>4</sub> than Si(H)<sub>3</sub>OH as the binding structures.<sup>32</sup>



**Scheme 2** Reactions involved in NO<sub>2</sub> adsorption on silica.

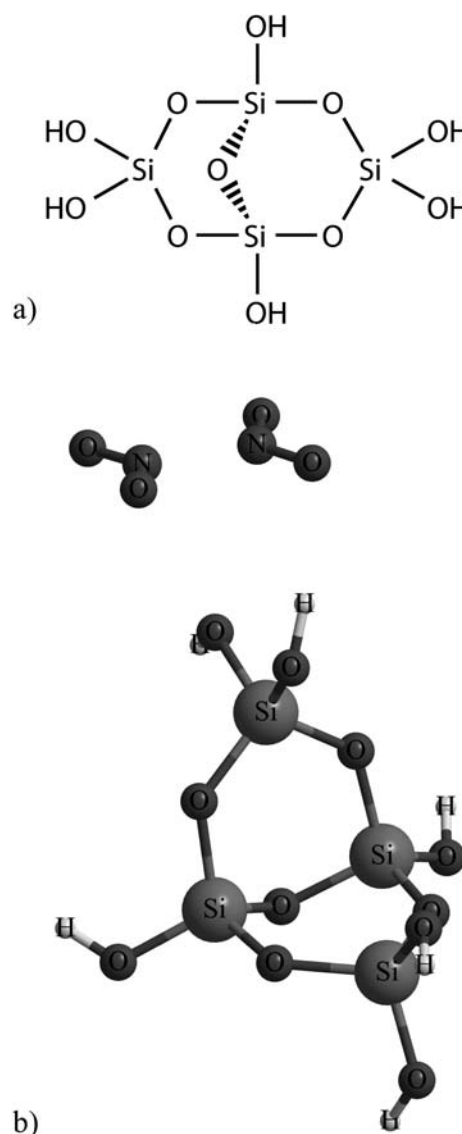


**Fig. 1** (a) Structure of Si<sub>4</sub>O<sub>11</sub>H<sub>6</sub>; (b) molecular modeling of interactions between adsorbed N<sub>2</sub>O<sub>4</sub> and Si<sub>4</sub>O<sub>11</sub>H<sub>6</sub> cluster. Full structural information is provided in supplementary information.

The treatment of hydrated silica-1073 with NO<sub>2</sub> ( $6.5 \times 10^{-8}$  mol NO<sub>2</sub> (g-silica s)<sup>-1</sup>) led to a total uptake of 75 μmol NO<sub>2</sub> g<sup>-1</sup> and the evolution of 25 μmol NO g<sup>-1</sup>. Neither HONO nor any other nitrogen-containing species were detected in the reactor effluent. We surmise that H<sub>2</sub>O facilitates the formation of NO *via* NO<sub>2</sub> disproportionation (reaction (4); Scheme 2), consistent with previous reports for NO<sub>2</sub> interactions with hydrated zeolites.<sup>40,43</sup> The lack of detectable HONO species reflects its rapid decomposition in the presence of the strong acids that accumulate as HNO<sub>3</sub> forms.<sup>41,44</sup> The similar NO<sub>2</sub> adsorption capacity on anhydrous and hydrated silica suggests that their NO<sub>2</sub> adsorption sites are similar in density and structure.

Scheme 1b summarizes the stoichiometry observed upon treating either hydrated or anhydrous silica-1073 with NO<sub>2</sub> in the experiments above, using the parameter  $\chi$ , which is defined as the amount of NO<sub>2</sub> consumed per NO formed in the gas phase. This parameter is useful below because it provides a unique

characteristic for identifying the type of  $\text{NO}_2$  storage site that is active within an experiment (*i.e.*,  $\chi$  is different for sites  $\text{B}_1$  and  $\text{B}_2$ ).

## 2. $\text{NO}_x$ adsorption via cascade reactions involving A (PTIO) and $\text{B}_1$ (silica-1073) sites

A reaction cascade for  $\text{NO}_x$  adsorption consisting of (i) NO oxidation to  $\text{NO}_2$  by physisorbed PTIO on silica (site A) followed by (ii)  $\text{NO}_2$  adsorption on silica (site  $\text{B}_1$ ) was examined by treating a physical mixture of PTIO supported on hydrated silica-1073 ( $200 \mu\text{mol g}^{-1}$ ;  $0.32 \text{ PTIO nm}^{-2}$ ) and hydrated silica-1073 with NO ( $3.3 \times 10^{-3} \text{ mol NO (PTIO s)}^{-1}$ ) in a packed bed. These experiments provide evidence for the effects of the relative concentration of type A and  $\text{B}_1$  sites on NO/PTIO stoichiometry ( $S$  in Scheme 1a).

The filled symbols in Fig. 2 represent the rates of NO consumption and  $\text{NO}_2$  formation for a sample with  $20 \mu\text{mol PTIO g}^{-1}$  in the adsorbent bed. The interactions of NO with PTIO led to a marked change in color from indigo-blue to orange, observed as a sharp band that advanced with time along the bed in the direction of flow. The saturation NO uptake was  $1.0 \pm 0.1$  NO per PTIO site, as expected from the ideal  $S$ -value; neither HONO nor  $\text{NO}_2$  were detected in the reactor effluent. Control experiments showed that PTIO sites are required for NO consumption, since no reaction products or adsorption were detected when hydrated or anhydrous silica-1073 were exposed to NO. These data are consistent with previous studies that report the value  $S$  of unity (*i.e.*, a ratio of unity for PTIO formed to PTIO consumed) upon treating a dilute PTIO on silica material (coverage below  $20 \mu\text{mol g}^{-1}$ ) with NO.<sup>25</sup>

The data in Fig. 2 suggest that  $\text{NO}_2$  adsorption on the hydrated silica-1073 sample proceeds without concurrent NO formation. Steps (2) and (3) in Scheme 2 do not occur in this case,

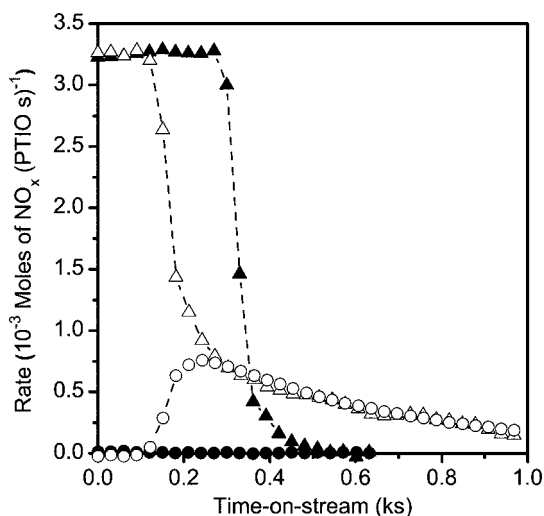


**Fig. 2** NO consumption (circles) and  $\text{NO}_2$  formation (triangles) rates during treatment of a physical mixture of PTIO supported on hydrated silica-1073 ( $200 \mu\text{mol PTIO g}^{-1}$ ) and hydrated silica-1073 with  $0.2 \text{ kPa NO}$  at  $3.3 \times 10^{-3} \text{ mol NO (PTIO s)}^{-1}$ . Filled symbols represent the sample consisting of  $20 \mu\text{mol PTIO g}^{-1}$  and open symbols represent the sample consisting of  $130 \mu\text{mol PTIO g}^{-1}$ . All data points are average of 32 infrared spectra.

in spite of the presence of hydrated silica-1073, because the total NO consumed per PTIO site would have otherwise been smaller than unity. These results reflect the reversible nature of reaction (4) in Scheme 2, which was previously shown to favor  $\text{HNO}_3$  decomposition at high NO concentrations (relative to  $\text{NO}_2$ ).<sup>45</sup> The high NO to  $\text{NO}_2$  molar ratio in the gas feed to the packed bed for the case of the experiment above (no  $\text{NO}_2$  in feed) similarly favors adsorption of the dimer  $\text{N}_2\text{O}_4$  without subsequent reaction with  $\text{H}_2\text{O}$  via steps (2) and (3) in Scheme 2.

Samples containing higher PTIO concentrations ( $60$  to  $130 \mu\text{mol PTIO g}^{-1}$ ) were also exposed to NO. These materials lack a sufficient number of  $\text{NO}_2$  adsorption ( $\text{B}_1$ -type) sites on silica to remove all the  $\text{NO}_2$  formed via NO oxidation on PTIO (A-type sites). NO reaction then occurs in two different regimes on mixtures with these higher PTIO concentrations. In the first regime ( $0$ – $0.12 \text{ ks}$ , Fig. 2), NO is rapidly and completely consumed but  $\text{NO}_2$  is not detected in the effluent. The second regime exhibits slower NO consumption and the detectable evolution of  $\text{NO}_2$ , as shown by the open symbols in Fig. 2 ( $0.12$ – $1 \text{ ks}$  on-stream). The transition coincides with the conversion of all PTIO sites in the bed, evident by the simultaneous completion of the indigo-blue to orange color change. The total NO uptake during the first regime was  $0.57 \pm 0.06 \text{ NO per PTIO}$  ( $75 \mu\text{mol NO g}^{-1}$ ) for the experiment with the highest PTIO concentration ( $130 \mu\text{mol PTIO g}^{-1}$ ); this NO/PTIO stoichiometry ( $S$ ) is much smaller than on the sample with the lowest PTIO content, which agreed with the expected value of unity. Such a low value of  $S$  cannot be explained by the contribution of NO formed upon  $\text{NO}_2$  reactions with hydrated silica-1073, because  $\text{NO}_2$  is stored on silica without the release of NO as a result of the low extent of the reversible reaction (4) in Scheme 2, when high NO to  $\text{NO}_2$  molar ratios are present in the gas phase.

Fig. 3 shows the general relation between NO/PTIO stoichiometry ( $S$ ) in the first regime and the concentration of PTIO sites in the packed bed. The titration of silica silanols by immobilized aminoxyl species (*vide infra*) led us to define the silica surface that contributes to  $\text{NO}_2$  binding as the amount of unfunctionalized silica within the bed. The NO uptake per PTIO site decreased monotonically with increasing PTIO site concentration, a trend that persisted when sites A and  $\text{B}_1$  were co-immobilized on the same support (see supplementary information). Taken together, these results suggest the involvement of a side reaction that consumes PTIO sites via reactions with the  $\text{NO}_2$  formed by NO oxidation, as a result of insufficient  $\text{B}_1$ -type  $\text{NO}_2$  storage sites. PTIO reacted with  $\text{NO}_2$  along the bed must become inactive towards NO (or react slowly with NO), resulting in smaller NO/PTIO uptakes. We explore this hypothesis of PTIO reactions with  $\text{NO}_2$  below by exposing PTIO supported on hydrated silica-1073 material to  $\text{NO}_2$  and measuring the number of reacted  $\text{NO}_2$ .

## 3. Reaction of $\text{NO}_2$ with PTIO supported on silica-1073

Literature reports of possible side reactions of  $\text{NO}_2$  with PTIO remain contradictory. Nadeau *et al.* concluded that dilute PTIO on silica did not react with  $\text{NO}_2$ ,<sup>25</sup> and a subsequent study found no reactions between gaseous  $\text{NO}_2$  and PTIO in aqueous solutions, even in excess  $\text{NO}_2$ , using spin resonance methods.<sup>46</sup> More recently, Goldstein *et al.* proposed a reversible reaction between  $\text{NO}_2$  and PTIO in aqueous solutions to form  $\text{PTIO}^+$  and

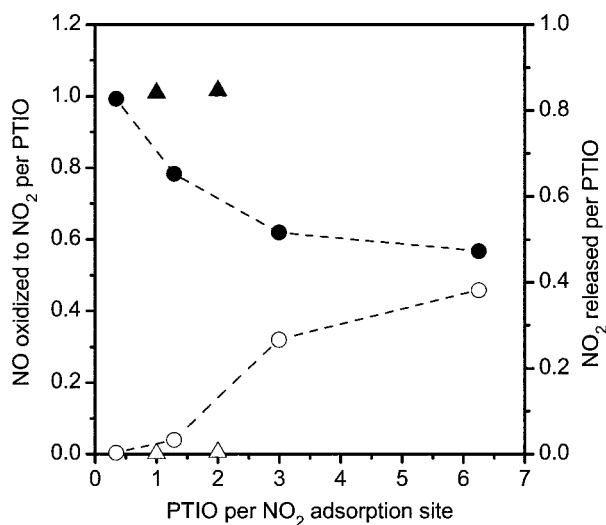


**Fig. 3** NO/PTIO stoichiometry of materials upon treatment with 0.2 kPa NO at  $3.3 \times 10^{-3}$  mol NO (PTIO s) $^{-1}$ . Circles represent a packed bed consisting of a physical mixture of PTIO supported on hydrated silica-1073 (200  $\mu\text{mol}$  PTIO  $\text{g}^{-1}$ ) and hydrated silica-1073 materials. Triangles represent a bed consisting of PTIO (100  $\mu\text{mol}$  PTIO  $\text{g}^{-1}$ ) and TEMPO (100  $\mu\text{mol}$  TEMPO  $\text{g}^{-1}$ ) species co-immobilized on the same silica support. Filled symbols represent NO oxidized to  $\text{NO}_2$  per PTIO within the regime of fast NO consumption, whereas open symbols represent total  $\text{NO}_2$  released per PTIO.  $\text{NO}_2$  adsorption on silica is assumed to occur *via* a non-oxidative mechanism at a capacity of 65  $\mu\text{mol}$   $\text{NO}_2$   $\text{g}^{-1}$ , as measured for silica-1073.

$\text{NO}_2^{-}$ .<sup>27,28</sup> The latter study also showed that  $\text{PTIO}^+$  can be reduced with either NO or  $\text{NO}_2^{-}$  to re-form PTIO, with  $\text{H}_2\text{O}$  providing the charge-balancing proton. The reduction of  $\text{PTIO}^+$  to PTIO by  $\text{NO}_2^{-}$  in aqueous solutions may account for the lack of detectable PTIO reactions with  $\text{NO}_2$  in the earlier studies.<sup>46</sup>

Treatment of PTIO sites supported on hydrated silica-1073 (200  $\mu\text{mol}$  PTIO  $\text{g}^{-1}$ ) with  $\text{NO}_2$  ( $2.8 \times 10^{-3}$  mol  $\text{NO}_2$  (PTIO s) $^{-1}$ ) led to an immediate color change from indigo-blue to dark orange, indicative of PTIO consumption. Nitrogen-containing species were not detected in the effluent until all PTIO sites were titrated and all traces of the blue color disappeared. During this time period of PTIO consumption (0–0.25 ks on-stream; Fig. 4), the total  $\text{NO}_2$  uptake per PTIO site was  $0.64 \pm 0.06$ . This uptake can be explained by  $\sim 85\%$  of the PTIO sites reacting *via* the sequence of reactions (5) and (6) (adding to reaction (7)) in Scheme 3 and requiring 0.5  $\text{NO}_2$ /PTIO, while the other  $\sim 15\%$  of the PTIO sites react *via* the sequence of reactions (8) and (9) (adding to reaction (10)) in Scheme 3 and requiring 1.0  $\text{NO}_2$ /PTIO. After all PTIO sites are consumed, NO and  $\text{NO}_2$  are detected in the effluent, apparently as the result of additional  $\text{NO}_2$  reactions with PTI *via* reaction (8), as well as plausible chemical reactions leading to the nitration of aromatic rings or to oxidation reactions that consume  $\text{NO}_2$ .

These conclusions were confirmed by the extraction of the species formed upon NO treatment of PTIO supported on hydrated silica-1073 to verify the occurrence of reactions between PTIO sites and the  $\text{NO}_2$  formed. The extracted species showed a significant content of polar species ( $\sim 30\%$  by weight) together with the less polar PTI fraction; these fractions were

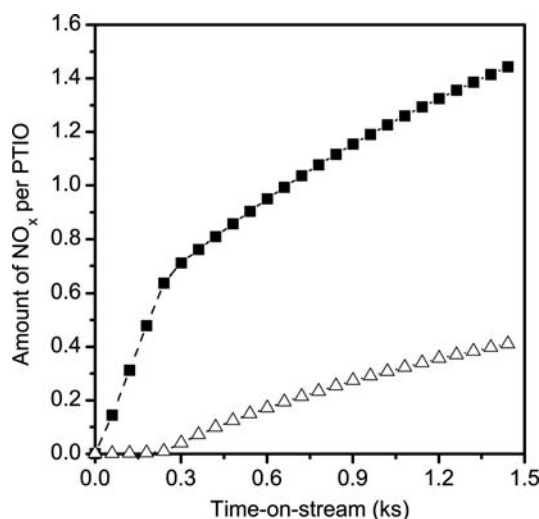
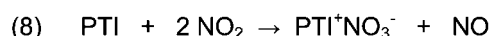
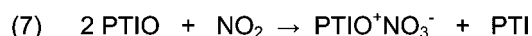
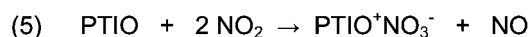


**Fig. 4**  $\text{NO}_2$  consumption (■) and NO formation ( $\Delta$ ) per PTIO site as a function of reaction time during treatment of silica-1073-supported PTIO (200  $\mu\text{mol}$  PTIO  $\text{g}^{-1}$ ) with 0.2 kPa  $\text{NO}_2$  at  $2.8 \times 10^{-3}$  mol  $\text{NO}_2$  (PTIO s) $^{-1}$ .

separated by chromatography (see supplementary information). These results are consistent with the formation of both PTI (non-polar) and  $\text{PTIO}^+\text{NO}_3^-$  (polar) species during reaction of NO with physisorbed PTIO on hydrated silica-1073 at high PTIO coverages, for which the scavenging of  $\text{NO}_2$  by silica adsorption sites is incomplete. Such a reaction forms oxoammonium nitrates and accounts for the decreased value  $S$  (Scheme 1a) measured for  $\text{NO}_x$  adsorption in packed beds consisting of PTIO concentrations at or above 60  $\mu\text{mol}$  PTIO  $\text{g}^{-1}$ . The  $S$ -value of unity observed on samples with the lowest PTIO concentration (20  $\mu\text{mol}$  PTIO  $\text{g}^{-1}$ ) indicates a lack of degradation of PTIO sites when excess  $\text{NO}_2$  storage sites are used to minimize local  $\text{NO}_2$  concentrations in the bed. Considering the fact that  $\text{NO}_2$  must diffuse out of a PTIO-functionalized silica particle before adsorbing to a hydrated silica-1073 particle within the packed bed, the observed  $S$ -value of unity further requires that the rate of internal mass transport be much faster than the intrinsic rate of  $\text{NO}_2$  reactions with immobilized PTI sites.

Having demonstrated the formation of  $\text{PTIO}^+\text{NO}_3^-$  upon treating PTIO with  $\text{NO}_2$ , it is possible to elucidate the second regime of slow reactions in Fig. 2. These slow processes must



**Scheme 3** Reactions involved in  $\text{NO}_2$  interaction with silica-supported PTIO.

consist of the reduction of the  $\text{PTIO}^+\text{NO}_3^-$  species by NO (see supplementary information), which is in agreement with earlier reports on the reduction of  $\text{PTIO}^+\text{NO}_2^-$  species by NO.<sup>27</sup>

#### 4. Reaction of $\text{NO}_2$ with TEMPO supported on hydrated silica-1073 (site $\text{B}_2$ )

The silica-supported PTIO system described in Section 2 functions selectively for  $\text{NO}_x$  storage only at PTIO bed concentration ( $20 \mu\text{mol g}^{-1}$ ) commensurate with the  $\text{NO}_2$  binding sites native to silica-1073 surface. The use of an organic active site for  $\text{NO}_2$  storage eliminates the need for excess silica by introducing a much higher density of binding sites than provided by geminal silanols at silica surfaces. This strategy may also prevent the formation of  $\text{HNO}_3$  on hydrated silica (reaction (4) in Scheme 2) and the potential corrosion and side reactions caused by the slow evolution of such species. TEMPO is used here as aminoxyl radical for  $\text{NO}_2$  reactions (site  $\text{B}_2$ ). We first describe the gas-phase species involved in  $\text{NO}_2$  adsorption on site  $\text{B}_2$  supported on hydrated silica-1073 and then explore the effects of PTIO and TEMPO bed concentrations on the NO/PTIO stoichiometry ( $S$ ) during NO oxidation to  $\text{NO}_2$ .

Reactions between  $\text{NO}_2$  and TEMPO are among the fastest  $\text{NO}_2$  reactions known.<sup>37</sup> It consumes two  $\text{NO}_2$  molecules per TEMPO and forms one oxoammonium nitrate ( $\text{TEMPO}^+\text{NO}_3^-$ ) and one NO (Scheme 1b).<sup>35</sup> This reaction has not been previously investigated on silica-supported TEMPO.  $\text{NO}_2$  adsorption on this material can occur *via* reactions with  $\text{B}_1$  sites on exposed silica surfaces (as in section 1) or on  $\text{B}_2$  TEMPO sites. Their relative contributions were examined by first treating TEMPO immobilized on hydrated silica-1073 ( $200 \mu\text{mol TEMPO g}^{-1}$ ;  $0.26 \text{ TEMPO nm}^{-2}$ ) with  $\text{NO}_2$  ( $1.4 \times 10^{-3} \text{ mol NO}_2 (\text{TEMPO s})^{-1}$ ). The data in Fig. 5 show that  $\text{NO}_2$  was not detected in the effluent until all TEMPO sites were titrated by  $\text{NO}_2$  (1.7 ks) with a stoichiometry of  $2.1 \pm 0.2 \text{ NO}_2/\text{TEMPO}$ . NO was detected

immediately upon  $\text{NO}_2$  introduction, consistent with the rapid formation of nitrates.<sup>35</sup> The irreversible formation of  $\text{TEMPO}^+\text{NO}_3^-$  species in these materials was confirmed by their infrared spectrum. A nearly symmetrical doublet band at 1413 and  $1336 \text{ cm}^{-1}$  was formed during contact of silica-473 supported TEMPO with  $\text{NO}_2$  (see supplementary information); this band is typical of nitrate anions.<sup>35</sup> The infrared spectrum of  $\text{TEMPO}^+\text{NO}_3^-$  did not change upon exposure to NO at ambient temperature, indicating that NO did not reduce  $\text{TEMPO}^+\text{NO}_3^-$  species and that interactions of  $\text{NO}_2$  with TEMPO are irreversible at these conditions. The ratio of  $\text{NO}_2$  consumption to NO formation rates ( $\chi$ ) during the time period for complete depletion of  $\text{NO}_2$  was constant at 2.0 (Fig. 5), consistent with the formation of stoichiometric  $\text{TEMPO}^+\text{NO}_3^-$  complexes *via* the reaction shown in Scheme 1b. This result requires that silica-based  $\text{NO}_2$  adsorption sites (corresponding to  $\text{B}_1$  in Scheme 1b) not participate in  $\text{NO}_2$  binding in TEMPO supported on hydrated silica-1073 materials, because such parallel reactions would lead to  $\chi$  values greater than two. This is consistent with the polar nature of TEMPO and  $\text{TEMPO}^+\text{NO}_3^-$  species attached to the same geminal silanol groups that would otherwise act as  $\text{NO}_2$  storage sites ( $\text{B}_1$  sites). Hydrogen-bonding interaction between aminoxyl species and silanols on the silica surface have been previously demonstrated *via* electron paramagnetic resonance spectroscopy.<sup>47</sup>

Samples with large ratios of surface silanols to TEMPO species led to detectable  $\text{NO}_2$  storage on silica-based  $\text{B}_1$ -type sites. In such cases, measured  $\chi$  values were greater than 2.0. For instance, the  $\chi$  value for TEMPO immobilized on hydrated silica-473 ( $200 \mu\text{mol g}^{-1}$ ;  $0.26 \text{ TEMPO nm}^{-2}$ ) with  $4.6 \text{ OH nm}^{-2}$  was 2.25. Contributions from  $\text{B}_1$ -type sites on silica-1073 were also evident on materials containing lower TEMPO surface concentration on silica-1073 (Fig. 6). The material with the largest excess of  $\text{NO}_2$  adsorption sites (corresponding to a TEMPO surface concentration of  $20 \mu\text{mol g}^{-1}$  on hydrated silica-1073) gave a  $\chi$  value of 2.75.

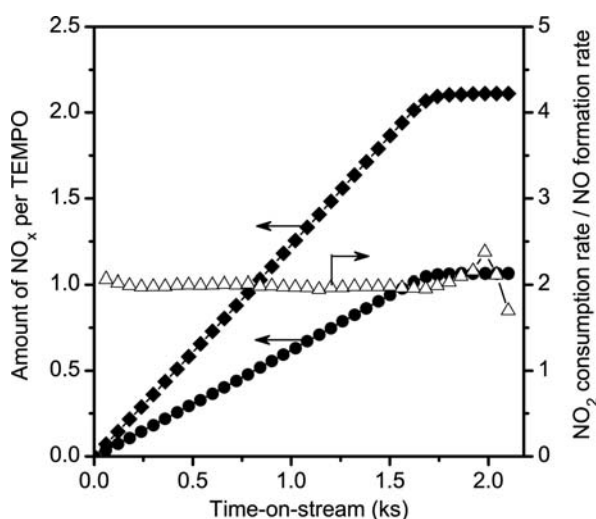


**Fig. 5**  $\text{NO}_2$  consumption (◆), NO formation (●) per TEMPO site, and  $\text{NO}_2$  consumption to NO formation rates ratio (△) as a function of reaction time of silica-1073-supported TEMPO ( $200 \mu\text{mol TEMPO g}^{-1}$ ) with  $0.2 \text{ kPa NO}_2$  at  $1.4 \times 10^{-3} \text{ mol NO}_2 (\text{TEMPO s})^{-1}$ .

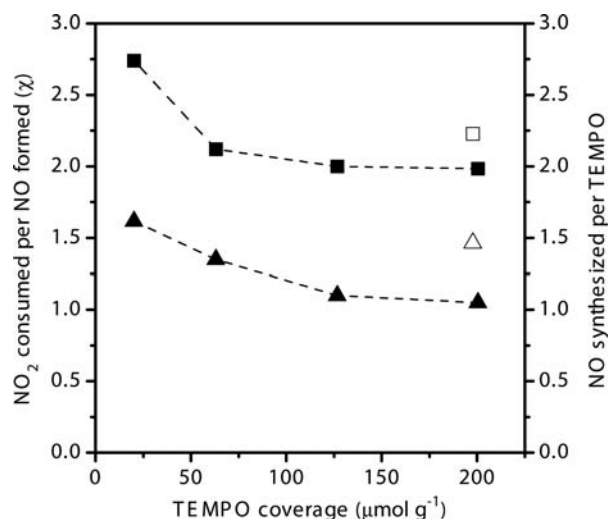
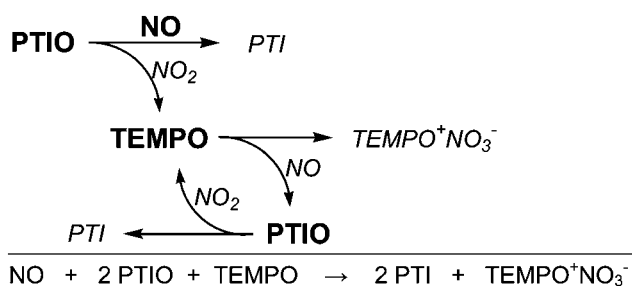


**Fig. 6** Coverage dependence of the average value of  $\chi$  (◆ □) and the number of NO released per TEMPO (▲ △) before breakthrough of  $\text{NO}_2$  (for example, before 1.7 ks in Fig. 5) for silica-1073 (filled symbols) and silica-473 (open symbols) supported TEMPO reacting with  $\text{NO}_2$ .

## 5. NO<sub>x</sub> adsorption via cascade reactions involving A (PTIO) and B<sub>2</sub> (TEMPO) sites

A functional system for NO<sub>x</sub> storage based on purely organic active sites was designed based on the data and conclusions shown in sections above. This system includes (i) NO oxidation on silica-supported PTIO (site A) to form NO<sub>2</sub> and (ii) NO<sub>2</sub> binding onto silica-supported TEMPO (site B<sub>2</sub>) in a form of oxoammonium TEMPO nitrate. This reaction cascade and its associated stoichiometry are represented in Scheme 4. This strategy requires the presence of two supported PTIO sites for each supported TEMPO site, so as to consume one equivalent of NO from the gas phase. This cascade assumes that silica acts as an inert support and lacks B<sub>1</sub>-type sites for NO<sub>2</sub> adsorption and that aminoxyl species fully titrate geminal silanols responsible for NO<sub>2</sub> binding, as shown in this study for silica-supported TEMPO adsorbents.



**Scheme 4** Cascade reactions network for NO<sub>x</sub> storage employing only organic active sites, consisting of (i) oxidation to NO<sub>2</sub> on PTIO site, and (ii) NO<sub>2</sub> storage by TEMPO site.

An equimolar physical mixture of PTIO (200 μmol PTIO g<sup>-1</sup>) and TEMPO (200 μmol TEMPO g<sup>-1</sup>) sites immobilized on separate hydrated silica-1073 aggregates (100 μmol g<sup>-1</sup> of each species in the mixture) was exposed to NO (3.1 × 10<sup>-3</sup> mol NO (aminoxyl s)<sup>-1</sup>). NO was removed to undetectable levels until all PTIO sites were reacted for a packed bed consisting of equal amounts of immobilized PTIO and TEMPO sites, which represents a two-fold excess of B<sub>2</sub>-type NO<sub>2</sub> adsorption sites according to the reaction-adsorption stoichiometry in Scheme 4. NO uptakes were 0.56 ± 0.05 NO per PTIO site (Fig. 7) and no NO<sub>2</sub> was detected in the effluent. A similar experiment with a packed bed containing a physical mixture of PTIO (200 μmol g<sup>-1</sup>) and TEMPO (200 μmol g<sup>-1</sup>) supported on separate hydrated silica-1073 particles at PTIO/TEMPO ratio equal to two led to similar NO/PTIO uptakes, consistent with the stoichiometry in Scheme 4 (Table 1).

PTIO and TEMPO sites can also be immobilized together on silica to prepare a material containing both NO oxidation and NO<sub>2</sub> storage sites within the same hydrated silica-1073 aggregates. We find, however, that there is no added benefit of co-immobilization *versus* physical mixtures of PTIO and TEMPO functionalized particles within the bed. The co-immobilized material containing 100 μmol g<sup>-1</sup> of each TEMPO and PTIO sites shows a similar NO/PTIO stoichiometry as co-mixed samples described above (Table 1; data in Fig. 7). All entries in Table 1 underscore the much more rapid rate of NO<sub>2</sub> reaction by immobilized TEMPO sites relative to its undesired reaction with

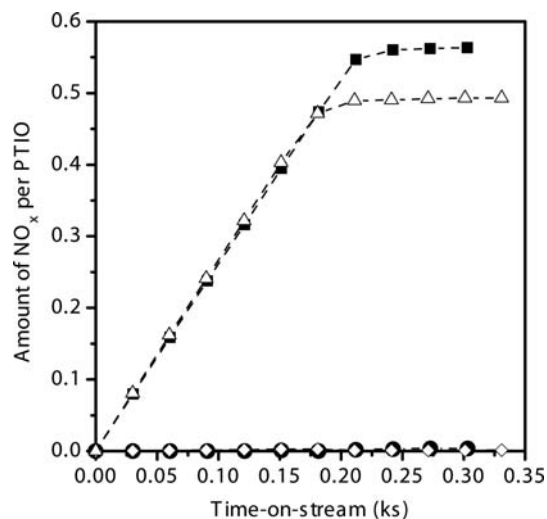


**Fig. 7** NO consumption (■ △) and NO<sub>2</sub> formation (● ◇) per PTIO site for co-immobilized (open symbols) and co-mixed (filled symbols) silica-1073 supported PTIO (100 μmol PTIO g<sup>-1</sup>) and TEMPO (100 μmol TEMPO g<sup>-1</sup>) reacting with 0.2 kPa NO at 3.1 × 10<sup>-3</sup> mol NO (aminoxyl s)<sup>-1</sup>. All data points are average of 32 infrared spectra.

**Table 1** NO consumption per PTIO site for physical mixture (TEMPO and PTIO physisorbed on separate hydrated silica-1073 support and mixed in packed bed) and co-immobilized (TEMPO and PTIO physisorbed together on the same hydrated silica-1073 support) reacting with 0.2 kPa NO at 3.1 × 10<sup>-3</sup> mol NO (aminoxyl s)<sup>-1</sup>

Entry	Packed bed	PTIO to TEMPO molar ratio	NO consumed per PTIO
1	Physical mixture	1 : 1	0.56 ± 0.05
2	Physical mixture	2 : 1	0.53 ± 0.05
3	Co-immobilized	1 : 1	0.50 ± 0.05
4	Co-immobilized	2 : 1	0.49 ± 0.05

either immobilized PTIO or PTI sites, because otherwise the measured NO consumed per PTIO would be significantly less than 0.5. The material consisting of PTIO and TEMPO co-immobilized on the same support in particular represents a versatile functional adsorbent for NO<sub>x</sub> in which all active sites are organic in nature and do not form the corrosive strong acids prevalent on inorganic adsorption sites, such as those present on unfunctionalized silica surfaces (Fig. 3).

## Conclusions

Silica-supported aminoxyl materials for NO<sub>x</sub> adsorption based on cascade reactions are investigated. The reaction sequence involves NO oxidation to NO<sub>2</sub> followed by NO<sub>2</sub> storage. One design uses PTIO sites as the oxidant and a dilute subset of silanols (geminal silanols) native to silica-1073 as the NO<sub>2</sub> storage site. NO/PTIO stoichiometry (*S*), however, decreases significantly away from unity due to degradation of PTIO sites by NO<sub>2</sub>, when less than the stoichiometric requirement of NO<sub>2</sub> storage sites is present. A completely organic-based NO<sub>x</sub> storage material can be synthesized using PTIO sites as NO oxidant and TEMPO sites for NO<sub>2</sub> storage. This material functions according to the predicted ideal stoichiometry, and implies that the

immobilization of aminoxyl sites on silica above a rather dilute critical coverage disables the ability of silica to act as NO<sub>2</sub> trap, presumably due to titration of the same silanols on silica that otherwise could serve as NO<sub>2</sub> storage sites.

## Experimental

### Preparation of the silica-supported aminoxyl radicals

Silica gel (Selecto Scientific, 32–63 μm particle size) with a surface area of 460 m<sup>2</sup> g<sup>-1</sup> was pretreated in He (Praxair, 99.999%) flowing at 0.1 cm<sup>3</sup> s<sup>-1</sup> g<sup>-1</sup> at 1073 K or 473 K for 8 h (denoted as silica-1073 or silica-473, respectively). This treatment provides a different amount and types of surface species that imply a various NO<sub>2</sub> adsorption binding strength and capacity. Surface area of silica was measured to be 380 m<sup>2</sup> g<sup>-1</sup> for silica-1073 and 460 m<sup>2</sup> g<sup>-1</sup> for silica-473. PTIO (TCI America, >98%) and TEMPO (Aldrich, 98%) were used as received. All silica samples were exposed to ambient atmosphere after thermal pretreatment step, unless otherwise noted. To prepare the material with necessary coverage the desirable amount of aminoxyl was dissolved in 5 cm<sup>3</sup> of dry dichloromethane (Aldrich, water <50 ppm) followed by adding 2 g of the silica gel to form a suspension. The indigo in case of PTIO and yellow in the case of TEMPO mixture was vigorously stirred under nitrogen atmosphere for 0.1 h at ambient temperature before the solvent was removed under reduced pressure and the resulting solid was dried under vacuum (20 Pa) for 2 h at ambient temperature. Co-immobilized PTIO and TEMPO on the same silica support were synthesized by the above-described procedure where total aminoxyl loading was 200 μmol g<sup>-1</sup>.

### Gas-phase reactions with NO and NO<sub>2</sub>

The reactions with NO and NO<sub>2</sub> were performed in a gas flow setup (see supplementary information). All gas mixtures were supplied by Praxair with a reported purity of 99.999% and balance gas of He. Mass flow controllers (MKS Instruments) were used to control the flows of 1% NO/10% Ar/He, 0.5% NO<sub>2</sub>/10% Ar/He, and He. The NO mixture was found to have an NO<sub>2</sub> impurity of 140 : 1 NO to NO<sub>2</sub>. Materials were supported on a 10 mm quartz frit within a quartz reactor. All reactions were conducted at 0.2 kPa NO<sub>x</sub>, 1 cm<sup>3</sup> s<sup>-1</sup> total flow rate and ambient temperature (ranging from 296 to 300 K). Heated process lines were used to transport all gases to the reactor and then to MKS 2030 Multigas FTIR analyzer to identify and quantify products. A gas cell with a path length of 2 cm and KBr windows were heated at 308 K during reaction experiments. The detection limit for nitrogen-containing species was 5 ppm. Scan averaging for infrared spectra was 64 with 0.5 cm<sup>-1</sup> wave number resolution for all reactions, except otherwise specified. The gas concentrations entering the reactor were measured *via* a reactor bypass. A dilution effect and NO<sub>2</sub> disproportionation on quartz wall of the reactor was subtracted from all measurements.

### Computational methodology

Quantum-chemical calculations were performed based on density functional theory using the B3LYP functional<sup>48</sup> along with the 6-311 + G(d,p) basis set. The calculations were

implemented using the software package *Gaussian 09*.<sup>49</sup> No symmetry restrictions were used in the calculations. Frequency calculations were performed for all stationary points using the same method and basis set as for geometry optimization experiments.

## Acknowledgements

The authors acknowledge Toyota Motor Co. for financial support and Dr Wang Feng for the design and construction of the experimental setup used in this study. The authors are grateful to Mr. Brian Weiss for helpful technical assistance and to Mr. Jamin Krinsky for valuable support during density functional theory calculations.

## References

- 1 A. S. Goldman, A. H. Roy, Z. Huang, R. Ahuja, W. Schinski and M. Brookhart, *Science*, 2006, **312**, 257.
- 2 K. Hamza, H. Schumann and J. Blum, *Eur. J. Org. Chem.*, 2009, 1502.
- 3 W. D. Fessner and C. Walter, *Angew. Chem., Int. Ed. Engl.*, 1992, **31**, 614.
- 4 R. Schoevaart, F. van Rantwijk and R. A. Sheldon, *J. Org. Chem.*, 2000, **65**, 6940.
- 5 R. Schoevaart and T. Kieboom, *Tetrahedron Lett.*, 2002, **43**, 3399.
- 6 S. K. Karmee, C. Roosen, C. Kohlmann, S. Lutz, L. Greiner and W. Leitner, *Green Chem.*, 2009, **11**, 1052.
- 7 B. A. Persson, A. L. E. Larsson, M. Le Ray and J. E. Backvall, *J. Am. Chem. Soc.*, 1999, **121**, 1645.
- 8 M. J. Climent, A. Corma, S. Iborra and M. Mifsud, *J. Catal.*, 2007, **247**, 223.
- 9 J. M. Robinson, C. E. Burgess, M. A. Bently, C. D. Brasher, B. O. Horne, D. M. Lillard, J. M. Macias, H. D. Mandal, S. C. Mills, K. D. O'Hara, J. T. Pon, A. F. Raigoza, E. H. Sanchez and J. S. Villarreal, *Biomass Bioenergy*, 2004, **26**, 473.
- 10 C. Zhao, Y. Kou, A. A. Lemonidou, X. B. Li and J. A. Lercher, *Angew. Chem., Int. Ed.*, 2009, **48**, 3987.
- 11 E. L. Margelefsky, R. K. Zeidan, V. Dufaud and M. E. Davis, *J. Am. Chem. Soc.*, 2007, **129**, 13691.
- 12 J. M. Notestein and A. Katz, *Chem.–Eur. J.*, 2006, **12**, 3954.
- 13 J. D. Bass, A. Solovoyov, A. J. Pascall and A. Katz, *J. Am. Chem. Soc.*, 2006, **128**, 3737.
- 14 J. D. Bass and A. Katz, *Chem. Mater.*, 2006, **18**, 1611.
- 15 M. Ojeda and E. Iglesia, *Chem. Commun.*, 2009, 352.
- 16 B. Chowdhury, J. J. Bravo-Suarez, N. Mimura, J. Q. Lu, K. K. Bando, S. Tsubota and M. Haruta, *J. Phys. Chem. B*, 2006, **110**, 22995.
- 17 B. Taylor, J. Lauterbach, G. E. Blau and W. N. Delgass, *J. Catal.*, 2006, **242**, 142.
- 18 C. Aprile, A. Corma, M. E. Domine, H. Garcia and C. Mitchell, *J. Catal.*, 2009, **264**, 44.
- 19 N. W. Cant, I. O. Y. Liu and M. J. Patterson, *J. Catal.*, 2006, **243**, 309.
- 20 B. M. Weiss and E. Iglesia, *J. Phys. Chem. C*, 2009, **113**, 13331.
- 21 J. D. Green and I. R. Harris, *Br. Pat.*, 1 592 157, 1981.
- 22 G. C. Koltsakis, P. A. Konstantinidis and A. M. Stamatelos, *Appl. Catal., B*, 1997, **12**, 161.
- 23 J. S. Stampler, D. J. Singel and J. Loscalzo, *Science*, 1992, **258**, 1898.
- 24 J. N. Pitts, K. A. Vancauwenberghe, D. Grosjean, J. P. Schmid, D. R. Fitz, W. L. Belser, G. B. Knudson and P. M. Hynds, *Science*, 1978, **202**, 515.
- 25 J. S. Nadeau and D. G. B. Boocock, *Anal. Chem.*, 1977, **49**, 1672.
- 26 O. Shimomura, K. Abe and M. Hirota, *J. Chem. Soc., Perkin Trans. 2*, 1988, 795.
- 27 S. Goldstein, A. Russo and A. Samuni, *J. Biol. Chem.*, 2003, **278**, 50949.
- 28 U. Samuni, Y. Samuni and S. Goldstein, *J. Am. Chem. Soc.*, 2010, **132**, 8428.
- 29 A. L. Goodman, G. M. Underwood and V. H. Grassian, *J. Phys. Chem. A*, 1999, **103**, 7217.
- 30 B. J. Finlayson-Pitts, L. M. Wingen, A. L. Sumner, D. Syomin and K. A. Ramazan, *Phys. Chem. Chem. Phys.*, 2003, **5**, 223.

- 31 R. Svensson, E. Ljungstrom and O. Lindqvist, *Atmos. Environ.*, 1987, **21**, 1529.
- 32 K. C. Thompson and P. Margey, *Phys. Chem. Chem. Phys.*, 2003, **5**, 2970.
- 33 W. S. Barney and B. J. Finlayson-Pitts, *J. Phys. Chem. A*, 2000, **104**, 171.
- 34 B. Djonev, B. Tsytarski, D. Klissurski and K. Hadjiivanov, *J. Chem. Soc., Faraday Trans.*, 1997, **93**, 4055.
- 35 G. Kaupp and J. Schmeyers, *J. Org. Chem.*, 1995, **60**, 5494.
- 36 Z. K. Ma, Q. T. Huang and J. M. Bobbitt, *J. Org. Chem.*, 1993, **58**, 4837.
- 37 S. Goldstein, A. Samuni and A. Russo, *J. Am. Chem. Soc.*, 2003, **125**, 8364.
- 38 E. G. Rozantsev, *Free nitroxyl radicals*, Plenum Press, 1970.
- 39 A. A. Tsyganenko, E. N. Storozheva, O. V. Manoilova, T. Lesage, M. Daturi and J. C. Lavalley, *Catal. Lett.*, 2000, **70**, 159.
- 40 M. Ahrens, O. Marie, P. Bazin and M. Daturi, *J. Catal.*, 2010, **271**, 1.
- 41 D. A. Syomin and B. J. Finlayson-Pitts, *Phys. Chem. Chem. Phys.*, 2003, **5**, 5236.
- 42 L. T. Zhuravlev, *Colloids Surf., A*, 2000, **173**, 1.
- 43 A. Grossale, I. Nova and E. Tronconi, *Catal. Lett.*, 2009, **130**, 525.
- 44 E. W. Kaiser and C. H. Wu, *J. Phys. Chem.*, 1977, **81**, 1701.
- 45 N. A. Saliba, H. Yang and B. J. Finlayson-Pitts, *J. Phys. Chem. A*, 2001, **105**, 10339.
- 46 T. Akaike, M. Yoshida, Y. Miyamoto, K. Sato, M. Kohno, K. Sasamoto, K. Miyazaki, S. Ueda and H. Maeda, *Biochemistry*, 1993, **32**, 827.
- 47 G. L. Markaryan and E. V. Lunina, *Zh. Fiz. Khim.*, 1996, **70**, 1670.
- 48 A. D. Becke, *J. Chem. Phys.*, 1993, **98**, 5648.
- 49 M. J. Frisch, G. W. Trucks, H. B. Schlegel, G. E. Scuseria, M. A. Robb, J. R. Cheeseman, G. Scalmani, V. Barone, B. Mennucci, G. A. Petersson, H. Nakatsuji, M. Caricato, X. Li, H. P. Hratchian, A. F. Izmaylov, J. Bloino, G. Zheng, J. L. Sonnenberg, M. Hada, M. Ehara, K. Toyota, R. Fukuda, J. Hasegawa, M. Ishida, T. Nakajima, Y. Honda, O. Kitao, H. Nakai, T. Vreven, J. J. A. Montgomery, J. E. Peralta, F. Ogliaro, M. Bearpark, J. J. Heyd, E. Brothers, K. N. Kudin, V. N. Staroverov, R. Kobayashi, J. Normand, K. Raghavachari, A. Rendell, J. C. Burant, S. S. Iyengar, J. Tomasi, M. Cossi, N. Rega, N. J. Millam, M. Klene, J. E. Knox, J. B. Cross, V. Bakken, C. Adamo, J. Jaramillo, R. Gomperts, R. E. Stratmann, O. Yazyev, A. J. Austin, R. Cammi, C. Pomelli, J. W. Ochterski, R. L. Martin, K. Morokuma, V. G. Zakrzewski, G. A. Voth, P. Salvador, J. J. Dannenberg, S. Dapprich, A. D. Daniels, J. B. O'FarkasForesman, J. V. Ortiz, J. Cioslowski, and D. J. Fox, *Gaussian, Inc.*, Wallingford, CT, 2009.